京都大学防災研究所年報　第42号　B-2　平成11年4月
Annuals of Disas. Prev. Res. Inst., Kyoto Univ., No. 42 B-2, 1999

A Numerical Model for Extended Boussinesq Equations in Generalized Curvilinear Coordinates and its Application to Solitary Wave Propagation in Curved Channel

Masatoshi YUHI*, Hajime ISHIDA* and Hajime MASE

*Department of Civil Engineering, Kanazawa University

Synopsis

A numerical model is developed for extended Boussinesq equations expressed in generalized curvilinear coordinate system. The model is applied to the study of solitary wave propagation through curved channels. The effects of channel width and incident wave height on the transmission and reflection properties are studied to understand the general features of solitary wave propagation. The maximum wave run-up at the outer vertical wall of channel is also investigated in order to estimate the possibility of wave overtopping at channel bends. Our numerical results show that the maximum run-up depends on one single dimensionless parameter proposed by Shi et al.(1998).

Keywords: Solitary wave; Curved Channel; Wave overtopping; Boussinesq equation; Coordinate Transformation

1. Introduction

It is essential to understand the dynamics of waves propagating in shallow water channels in order to estimate the wave-overtopping quantity and to make effective countermeasures against it. From this point of view, the problems of solitary wave propagation in straight channels have been studied theoretically, experimentally and numerically by a lot of researchers. On the contrary, only a few research works can be found which treat the propagation of solitary wave in curved channels. From engineering aspects, however, rivers, harbors and canals have often winding turns in direction. It is therefore important to understand the features of solitary wave propagation in curved channels.

In this paper, a numerical model is developed for computing the propagation of shallow water waves through channels of arbitrary shape. The extended Boussinesq equations transformed into generalized curvilinear coordinate system are adopted as governing equations and are solved by using finite difference method. The model is applied to the study of long wave propagation in curved channels. The properties of transmission and reflection of a solitary wave are examined for a circular channel of constant width and water-depth. The effects of channel width and incident wave height on maximum run-up at the outer channel wall are investigated in detail. An attempt to correlate the maximum wave run-up with a dimensionless parameter is also made.

In the next chapter, the governing equations and the necessary boundary conditions are summarized. In chapter three, we explain the method of numerical calculation. The numerical results for curved channels are shown and discussed in chapter four. Conclusions are summarized in chapter five.

2. Mathematical Formulation

2.1 Governing Equations

The extended Boussinesq equations derived by Nwogu(1993) are given in dimensionless form by

$$\frac{\partial \zeta}{\partial t}+\nabla\cdot\left[(h+\varepsilon\zeta)u\right]+\mu^2\nabla\cdot\left[\left(\frac{z^2}{2}-\frac{h^2}{6}\right)h\nabla(\nabla\cdot u)\right]$$
$$+\mu^2\nabla\cdot\left[\left(z+\frac{h}{2}\right)h\nabla(\nabla\cdot(hu))\right]=0 \quad (1)$$

$$\frac{\partial u}{\partial t}+\nabla\zeta+\varepsilon(u\cdot\nabla)u$$
$$+\mu^2\left[\left(\frac{z^2}{2}\right)\nabla\left(\nabla\cdot\left(\frac{\partial \mathbf{u}}{\partial t}\right)\right)+z\nabla\left(\nabla\cdot\left(h\frac{\partial \mathbf{u}}{\partial t}\right)\right)\right]=0 \quad (2)$$

where ζ = surface elevation, h = local water depth, $u=(u,v)$ = horizontal velocity at an arbitrary depth, z. Two dimensionless parameters, which represent the effects of dispersion and nonlinearity, respectively, are defined as follows:

$$\mu=\bar{h}_0/\bar{\lambda}_0 \quad (3)$$

$$\varepsilon=\bar{a}_0/\bar{h}_0 \quad (4)$$

where $\bar{h}_0$ is the representative water depth, $\bar{\lambda}_0$ is the incident wave length and $\bar{a}_0$ is the incident wave amplitude, respectively, and over-bar denotes dimensional quantities. The definitions of the non-dimensional quantities are shown in Appendix.

These equations can be rearranged as

$$\frac{\partial \zeta}{\partial t}=E(\zeta,u,v) \quad (5)$$

$$\frac{\partial U}{\partial t}=F(\zeta,u,v) \quad (6)$$

$$\frac{\partial V}{\partial t}=G(\zeta,u,v) \quad (7)$$

where

$$U=u+\mu^2h\left(b_1h\frac{\partial^2 u}{\partial x^2}+b_2\frac{\partial^2(hu)}{\partial x^2}\right) \quad (8)$$

$$V=v+\mu^2h\left(b_1h\frac{\partial^2 v}{\partial y^2}+b_2\frac{\partial^2(hv)}{\partial y^2}\right) \quad (9)$$

are treated as simple variables in time-stepping procedure. The remaining terms, E, F and G, are functions of ζ, u and v that are defines as

$$E=-\frac{\partial}{\partial x}\left[(h+\varepsilon\zeta)u\right]-\frac{\partial}{\partial y}\left[(h+\varepsilon\zeta)v\right]$$
$$-\mu^2\frac{\partial}{\partial x}\left[a_1h^3\left(\frac{\partial^2 u}{\partial x^2}+\frac{\partial^2 v}{\partial x\partial y}\right)+a_2h^2\left(\frac{\partial^2 hu}{\partial x^2}+\frac{\partial^2 hv}{\partial x\partial y}\right)\right]$$
$$-\mu^2\frac{\partial}{\partial y}\left[a_1h^3\left(\frac{\partial^2 v}{\partial y^2}+\frac{\partial^2 u}{\partial x\partial y}\right)+a_2h^2\left(\frac{\partial^2 hv}{\partial y^2}+\frac{\partial^2 hu}{\partial x\partial y}\right)\right] \quad (10)$$

$$F=-\frac{\partial \zeta}{\partial x}-\varepsilon\left(u\frac{\partial u}{\partial x}+v\frac{\partial u}{\partial y}\right)$$
$$-\mu^2h\frac{\partial}{\partial t}\left(b_1h\frac{\partial^2 v}{\partial x\partial y}+b_2\frac{\partial^2 hv}{\partial x\partial y}\right) \quad (11)$$

$$G=-\frac{\partial \zeta}{\partial y}-\varepsilon\left(u\frac{\partial v}{\partial x}+v\frac{\partial v}{\partial y}\right)$$
$$-\mu^2h\frac{\partial}{\partial t}\left(b_1h\frac{\partial^2 u}{\partial x\partial y}+b_2\frac{\partial^2 hu}{\partial x\partial y}\right) \quad (12)$$

The constants a_1, a_2, b_1 and b_2 are given by

$$a_1=\beta^2/2-1/6, a_2=\beta+1/2, b_1=\beta^2/2, b_2=\beta \quad (13)$$

where $\beta = z/h$.

2.2 Coordinate Transformation

Since the precise expression of the channel geometry is essential to accurately calculate the wave propagation in curved channels, the following coordinate transformation is introduced to fit the numerical domain to the channel boundary:

$$x=x(\xi,\eta), y=y(\xi,\eta) \quad (14)$$

where (x,y) are variables in physical plane and (ξ,η) are those in transformed (i.e. computational) plane. From Eq.(14), we can write first order partial derivatives in the following way:

$$\frac{\partial}{\partial x}=a_{11}\frac{\partial}{\partial \xi}+a_{21}\frac{\partial}{\partial \eta} \quad (15)$$

$$\frac{\partial}{\partial y}=a_{12}\frac{\partial}{\partial \xi}+a_{22}\frac{\partial}{\partial \eta} \quad (16)$$

in which a_{ij} $(i=1,2; j=1,2)$ are defined as

$$\left.\begin{aligned} a_{11}&=\frac{1}{J}\frac{\partial y}{\partial \eta}, \; a_{21}=-\frac{1}{J}\frac{\partial y}{\partial \xi}\\ a_{12}&=-\frac{1}{J}\frac{\partial x}{\partial \eta}, \; a_{22}=\frac{1}{J}\frac{\partial x}{\partial \xi}\end{aligned}\right\} \quad (17)$$

and

$$J=\frac{\partial x}{\partial \xi}\frac{\partial y}{\partial \eta}-\frac{\partial x}{\partial \eta}\frac{\partial y}{\partial \xi} \quad (18)$$

Applying these operators again to obtain second derivatives yields

$$\frac{\partial^2}{\partial x^2}=a_{11}^2\frac{\partial^2}{\partial \xi^2}+2a_{11}a_{21}\frac{\partial^2}{\partial \xi\partial \eta}+a_{21}^2\frac{\partial^2}{\partial \eta^2}$$
$$+b_{11}\frac{\partial}{\partial \xi}+b_{12}\frac{\partial}{\partial \eta} \quad (19)$$

$$\frac{\partial^2}{\partial x\partial y}=a_{11}a_{12}\frac{\partial^2}{\partial \xi^2}+(a_{11}a_{22}+a_{21}a_{12})\frac{\partial^2}{\partial \xi\partial \eta}+a_{21}a_{22}\frac{\partial^2}{\partial \eta^2}$$
$$+b_{21}\frac{\partial}{\partial \xi}+b_{22}\frac{\partial}{\partial \eta} \quad (20)$$

$$\frac{\partial^2}{\partial y^2} = a_{12}{}^2 \frac{\partial^2}{\partial \xi^2} + 2a_{12}a_{22}\frac{\partial^2}{\partial \xi\,\partial \eta} + a_{22}{}^2 \frac{\partial^2}{\partial \eta^2}$$

$$+ b_{31}\frac{\partial}{\partial \xi} + b_{32}\frac{\partial}{\partial \eta} \tag{21}$$

where b_{ij} $(i = 1,3;\ j = 1,2)$ are given by

$$\left.\begin{aligned} b_{11} &= -a_{12}c_{11} - a_{11}c_{12} \\ b_{12} &= -a_{22}c_{11} - a_{21}c_{12} \\ b_{21} &= c_{21}/J \\ b_{22} &= c_{22}/J \\ b_{31} &= -a_{12}c_{31} - a_{11}c_{32} \\ b_{32} &= -a_{22}c_{31} - a_{21}c_{32} \end{aligned}\right\} \tag{22}$$

and

$$\left.\begin{aligned} c_{11} &= a_{11}{}^2\frac{\partial^2 y}{\partial \xi^2} + 2a_{11}a_{21}\frac{\partial^2 y}{\partial \xi\,\partial \eta} + a_{21}{}^2\frac{\partial^2 y}{\partial \eta^2} \\ c_{12} &= a_{11}{}^2\frac{\partial^2 x}{\partial \xi^2} + 2a_{11}a_{21}\frac{\partial^2 x}{\partial \xi\,\partial \eta} + a_{21}{}^2\frac{\partial^2 x}{\partial \eta^2} \\ c_{21} &= a_{22}\frac{\partial^2 y}{\partial \eta^2} + a_{12}\frac{\partial^2 y}{\partial \xi\,\partial \eta} - a_{11}a_{12}\frac{\partial J}{\partial \xi} - a_{11}a_{22}\frac{\partial J}{\partial \eta} \\ c_{22} &= -a_{12}\frac{\partial^2 y}{\partial \xi^2} - a_{22}\frac{\partial^2 y}{\partial \xi\,\partial \eta} - a_{21}a_{12}\frac{\partial J}{\partial \xi} - a_{21}a_{22}\frac{\partial J}{\partial \eta} \\ c_{31} &= a_{12}{}^2\frac{\partial^2 y}{\partial \xi^2} + 2a_{12}a_{22}\frac{\partial^2 y}{\partial \xi\,\partial \eta} + a_{22}{}^2\frac{\partial^2 y}{\partial \eta^2} \\ c_{32} &= a_{12}{}^2\frac{\partial^2 x}{\partial \xi^2} + 2a_{12}a_{22}\frac{\partial^2 x}{\partial \xi\,\partial \eta} + a_{22}{}^2\frac{\partial^2 x}{\partial \eta^2} \end{aligned}\right\} \tag{23}$$

2.3 Boundary Conditions

Three types of boundary conditions are necessary for the problem treated in this study; namely (i) impermeable, reflective vertical wall; (ii) incident wave boundary; and (iii) transmitting boundary. For each type of these boundaries, we impose the following conditions which are proposed by Wei and Kirby(1995).

For a general reflective boundary with an outward normal vector $\mathbf{n}$, we require

$$\mathbf{u}\cdot\mathbf{n} = 0 \tag{24}$$

$$\nabla\zeta\cdot\mathbf{n} = 0 \tag{25}$$

$$\frac{\partial u_T}{\partial n} = 0 \tag{26}$$

in which u_T is the velocity component tangent to the boundary. At incident wave boundary, we specify the entire signal of ζ and $\mathbf{u}$ from the analytical solution of the extended Boussinesq equations. Finally, the radiation condition combined with wave damping layer is used at the transmitting boundary.

3. Numerical Implementation

Wei and Kirby(1995) developed a high-order numerical code for extended Boussinesq equations in Cartesian coordinate system. In this study, we slightly modified their numerical scheme and extend it for generalized curvilinear coordinate system.

3.1 Time stepping procedure

A fourth-order predictor-corrector scheme is adopted for time-stepping procedure. The predictor step is the third-order explicit Adams-Bashforth scheme (Press et al., 1989) given by

$$\zeta_{i,j}^{n+1^*} = \zeta_{i,j}^{n} + \frac{\Delta t}{12}\left(23E_{i,j}^{n} - 16E_{i,j}^{n-1} + 5E_{i,j}^{n-2}\right) \tag{27}$$

$$U_{i,j}^{n+1^*} = U_{i,j}^{n} + \frac{\Delta t}{12}\left(23F_{i,j}^{n} - 16F_{i,j}^{n-1} + 5F_{i,j}^{n-2}\right) \tag{28}$$

$$V_{i,j}^{n+1^*} = V_{i,j}^{n} + \frac{\Delta t}{12}\left(23G_{i,j}^{n} - 16G_{i,j}^{n-1} + 5G_{i,j}^{n-2}\right) \tag{29}$$

where all information on the right hand side is known from previous calculations. Although the evaluation of ζ is straightforward, the evaluation of u and v requires solutions of Eqs.(8) and (9), that are described in generalized coordinates as

$$U = u + \mu^2 b_1 h^2\left(a_{11}{}^2\frac{\partial^2 u}{\partial \xi^2} + 2a_{11}a_{21}\frac{\partial^2 u}{\partial \xi\,\partial \eta} + a_{21}{}^2\frac{\partial^2 u}{\partial \eta^2}\right.$$

$$\left. b_{11}\frac{\partial u}{\partial \xi} + b_{12}\frac{\partial u}{\partial \eta}\right) + \mu^2 b_2 h\left(a_{11}{}^2\frac{\partial^2 hu}{\partial \xi^2} + 2a_{11}a_{21}\frac{\partial^2 hu}{\partial \xi\,\partial \eta}\right.$$

$$\left. + a_{21}{}^2\frac{\partial^2 hu}{\partial \eta^2} + b_{11}\frac{\partial hu}{\partial \xi} + b_{12}\frac{\partial hu}{\partial \eta}\right) \tag{30}$$

$$V = v + \mu^2 b_1 h^2\left(a_{12}{}^2\frac{\partial^2 v}{\partial \xi^2} + 2a_{12}a_{22}\frac{\partial^2 v}{\partial \xi\,\partial \eta} + a_{22}{}^2\frac{\partial^2 v}{\partial \eta^2}\right.$$

$$\left. b_{31}\frac{\partial v}{\partial \xi} + b_{32}\frac{\partial v}{\partial \eta}\right) + \mu^2 b_2 h\left(a_{12}{}^2\frac{\partial^2 hv}{\partial \xi^2} + 2a_{12}a_{22}\frac{\partial^2 hv}{\partial \xi\,\partial \eta}\right.$$

$$\left. + a_{22}{}^2\frac{\partial^2 hv}{\partial \eta^2} + b_{31}\frac{\partial hv}{\partial \xi} + b_{32}\frac{\partial hv}{\partial \eta}\right) \tag{31}$$

These equations are finite-differenced and solved numerically by using successive over relaxation (S.O.R.) method. After obtained the predicted values of surface elevation and horizontal velocities, the corresponding derivatives in Eqs.(10) to (12) are calculated from Eqs.(15) to (23).

The corrector scheme is the fourth-order implicit Adams-Moulton method, which is given by

$$\zeta_{i,j}^{n+1} = \zeta_{i,j}^{n} + \frac{\Delta t}{24}\left(9E_{i,j}^{n+1^*} + 19E_{i,j}^{n} - 5E_{i,j}^{n-1} + E_{i,j}^{n-2}\right) \quad (32)$$

$$U_{i,j}^{n+1} = U_{i,j}^{n} + \frac{\Delta t}{24}\left(9F_{i,j}^{n+1^*} + 19F_{i,j}^{n} - 5F_{i,j}^{n-1} + F_{i,j}^{n-2}\right) \quad (33)$$

$$V_{i,j}^{n+1} = V_{i,j}^{n} + \frac{\Delta t}{24}\left(9G_{i,j}^{n+1^*} + 19G_{i,j}^{n} - 5G_{i,j}^{n-1} + G_{i,j}^{n-2}\right) \quad (34)$$

The corrector step is iterated until the error between two successive iterations reaches a required criterion. The error is defined as

$$\Delta f = \frac{\sum_{i,j}\left|f_{i,j}^{n+1} - f_{i,j}^{n+1^*}\right|}{\sum_{i,j}\left|f_{i,j}^{n+1}\right|} \quad (35)$$

in which f denotes each of the three dependent variables, ζ, u, v, and ()* denotes the previous estimate. The corrector step is iterated if any of the value of Δf exceeds 0.0001. Then the same procedure is applied to the next time step.

3.2 Spatial discretization

For first-order spatial derivatives, we adopt the fourth-order central difference given by

$$\left.\begin{aligned}\frac{\partial f}{\partial \xi} &\approx \frac{-f_{i+2,j} + 8f_{i+1,j} - 8f_{i-1,j} + f_{i-2,j}}{12\Delta\xi} \\ \frac{\partial f}{\partial \eta} &\approx \frac{-f_{i,j+2} + 8f_{i,j+1} - 8f_{i,j-1} + f_{i,j-2}}{12\Delta\eta}\end{aligned}\right\} \quad (36)$$

On the other hand, second-order spatial derivatives are approximated by second-order central differences that are described as

$$\left.\begin{aligned}\frac{\partial^2 f}{\partial \xi^2} &\approx \frac{f_{i+1,j} - 2f_{i,j} + f_{i-1,j}}{(\Delta\xi)^2} \\ \frac{\partial^2 f}{\partial \eta^2} &\approx \frac{f_{i,j+1} - 2f_{i,j} + f_{i,j-1}}{(\Delta\eta)^2} \\ \frac{\partial^2 f}{\partial \xi\, \partial \eta} &\approx \frac{f_{i+1,j+1} - f_{i+1,j-1} - f_{i-1,j+1} + f_{i-1,j-1}}{4\Delta\xi\,\Delta\eta}\end{aligned}\right\} \quad (37)$$

All the equations are discretized on an unstaggered grid.

3.3 Verification of the numerical scheme

In order to examine the accuracy of the numerical scheme adopted in this study, we investigate the propagation of a solitary wave in a straight channel of constant depth and width. The total length of the channel is set to be 100h and the channel width is set to be 5h. A solitary wave is generated at the left boundary according to the analytical solitary wave solution derived by Wei and Kirby(1995). The wave is transmitted at the right boundary. The corresponding values of ε and μ are 0.3 and 0.071, respectively. For solitary waves, we define the effective wave length λ_e as the wave length within which the wave elevation everywhere is larger than 1% of its amplitude.

The spatial profiles of the solitary wave are described in Fig.1 for various time instants. The results shows that initial waveform undergo small evolution, which results in a slightly (about 3%) larger wave height. This is partially because the analytical solution used at the incident boundary is only asymptotically equivalent to the numerical model. In fig.2, solitary wave profiles are compared at two widely separated instances in time. The two waveforms are translated by an amount predicted by the analytical phase speed. The results show that the wave propagates for a long distance (at least 50 water depths) without any distortion except for the initial small evolution. The error in phase celerity was found to be less than 0.6%. These results thus validate the reasonably high accuracy of the numerical scheme.

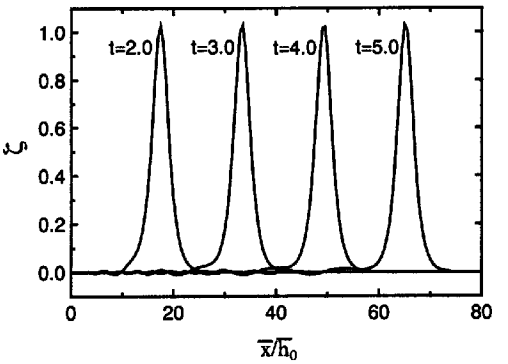

Fig.1 Spatial profiles of solitary wave at the centerline of the channel for various time steps

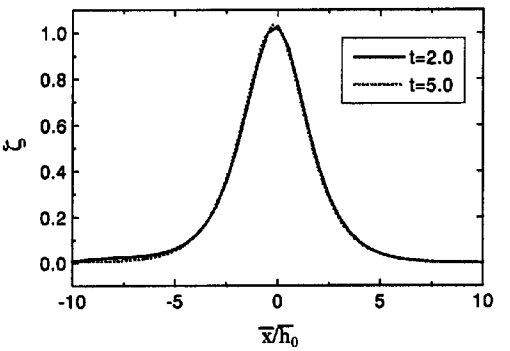

Fig.2 Comparison of solitary wave shapes at t=2.0 and t=5.0

4. Results and Discussions

The geometry of the curved channel model is shown in Fig.3 schematically. In the numerical simulations, all the channels have a circular corner of constant inner radius of 10 water depths with the upstream and downstream legs of 50 water depths in length. The water depth and the channel width are uniform throughout the channel. In the following, the effects of relative channel width, $\overline{W}/\overline{h}_0$, and the incident wave nolinearity, ε, on solitary wave propagation are investigated in detail. The test conditions are summarized in Table 1.

4.1 General Features of Transmission and Reflection of Solitary Waves

The numerical results for a solitary wave of small incident wave amplitude through a narrow channel (Case A-1) are shown in Fig.4 (a)-(e). These figures show the evolution of the solitary wave at various time instants through the circular bend. When the incident wave arrives at the curved section, the wave is nearly one-dimensional and the initial wave profile is almost completely preserved. During its passage through the bend, however, the wave tilts higher outward against the outer wall. The difference of wave height in radial direction keeps balance with the centrifugal force. In such a case, the wave propagates faster in outer region, because the phase speed of the solitary wave increases with the increase of its wave height. The increased phase speed compensates for the increase of the propagation length along the wall in outer region, which result in radially straight crest line. After passing through the bend, the wave recovers its initial shape quickly to make the wave crest uniform

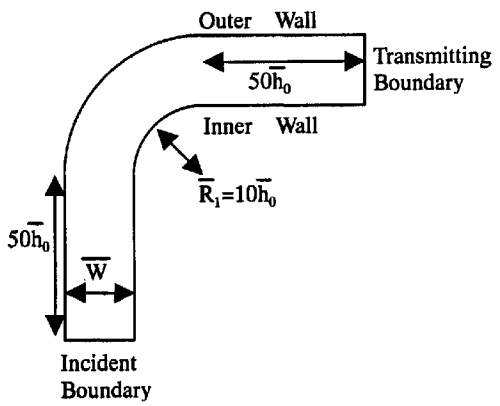

Fig.3 Geometry of the curved channel

Table 1 Test conditions

Case No.	ε	$\overline{W}/\overline{h}_0$	μ	$\overline{W}/\overline{\lambda}_e$
A-1	0.05	5.0	0.032	0.16
A-2	0.10	5.0	0.044	0.22
A-3	0.15	5.0	0.053	0.26
A-4	0.20	5.0	0.060	0.30
A-5	0.25	5.0	0.066	0.33
B-1	0.05	10.0	0.032	0.32
B-2	0.10	10.0	0.044	0.44
B-3	0.15	10.0	0.053	0.53
B-4	0.20	10.0	0.060	0.60
B-5	0.25	10.0	0.062	0.66
C-1	0.05	20.0	0.032	0.63
C-2	0.10	20.0	0.044	0.88
C-3	0.15	20.0	0.053	1.06
C-4	0.20	20.0	0.060	1.20
C-5	0.25	20.0	0.066	1.32

across the channel. It is seen from these results that the solitary wave is almost completely transmitted with little reflection in narrow circular channels. These results are consistent with the works by Shi et al.(1995).

The numerical results for solitary wave of incident wave amplitude $\varepsilon = 0.15$ through the channel with moderate width (Case B-3) are shown in Fig.5(a)-(e). Just after the solitary wave enters into the circular part, the wave tilts higher outward against the outer wall. This shape is similar to the one recognized in the narrow channel results. During its passage through the bend, however, the transmission and reflection of the solitary wave in wider channel are different from those in narrow channel. As the wave propagates through the circular bend, the wave tends to diffract near inner wall although the wave tends to travel straight near outer wall. Consequently, the solitary wave becomes no longer radially straight and the transmitted wave loses its initial shape. The wave height of diffracted wave decreases gradually as it travels. At the outer wall, the wave height increases as the solitary wave travels through the channel. The maximum wave height is attained at the middle of the outer wall and then the wave is reflected into inner region. After the wave passed through the bend, the reflected wave propagates toward the inner wall. As a result, the wave height at the inner wall becomes higher, in turn. The maximum wave height at the inner wall is, however, much smaller than that attained at the outer wall. Since the reflected wave propagates much faster along the wall than the diffracted wave, the

former catches up with the latter to merge into one wave in the final stage of wave transformation. From the comparison between the narrow channel results and the results with moderate channel width, it is found that the amplitude of the transmitted wave decreases as the channel width increases.

Numerical results for the solitary wave of a large wave height through wide channel (Case C-5) are shown in Fig.6(a)-(h). These results are quite different from those in narrow channels. The main features seen in the moderate width case are enhanced, namely we observe that the wave transformation and the reflection at the outer channel wall becomes much stronger in wide channel. The maximum wave height at the outer wall reaches almost 200% of the incident wave height in this case.

When waves incident to a straight wall with small incident angle, the regular type of reflection gives way to another type of reflection, which is called 'Mach reflection' (e.g. Tanaka;1993). In Mach reflection, three kinds of waves are present near the wall: the incident wave, the reflected wave and a wave propagating along the wall called the stem wave. The wave height of stem wave can grow significantly along the wall. In the winding part of curved channel, waves incident to the outer wall with small angle, and therefore we may expect that the same situation happens as mentioned above. The situation for curved channel is, however, more complicated because the geometry of the wall is not straight and the incident angle increases gradually as the wave propagates. According to the previous works concerning the Mach reflection on a straight wall, the development of Mach stem is limited in the case of small incident angle. Hence, the gradual increase of the incident angle to the wall may prevent the Mach stem development. In addition, Mach stem development is quite a slow phenomena and therefore it takes very long time for Mach reflection to be attained. For these reasons, it is probable that the Mach reflection can be seen only in very wide channels. The wave patterns shown in Fig.6(d)-(f) are similar to the ones in Mach reflection at the straight wall, but it cannot be decided, at present, whether this may be called a Mach reflection or not. Further investigations and improvement of the numerical model to account for the strong nonlinearity (e.g. extension to the fully nonlinear Boussinesq equations (Wei et al.;1997)), are necessary for precise discussion.

4.2 Maximum Wave Run-up at outer wall

It is very important to predict the maximum wave height at channel walls in order to prevent the wave overtopping from channels. In Fig.7, the maximum wave height normalized by the incident wave height is plotted as a function of ε for various values of relative channel width. As ε increases, the wave run-up gradually increases and asymptotes to a constant value for each case. It is also seen that the maximum wave height is an increasing function of the channel width. We also investigated the location at which the maximum wave height is attained. The results are shown in Fig.8. In the case of a narrow channel, the position gradually moves downstream as ε increases. For wider channels, however, the location is independent of ε and takes almost the constant value of 48 degree and 53 degree, respectively. In general, the location moves to the downstream direction as the channel width increases.

Shi et al.(1998) proposed a dimensionless parameter,

$$\alpha = \overline{W} / \overline{\lambda}_e \tag{38}$$

which characterizes the solitary wave propagation in straight channel with sharp-cornered bend. They found that the transmission and reflection properties of solitary waves in such channels depend on this dimensionless parameter. It deserves consideration whether this parameter is also effective for smoothly curved channels or not. The maximum wave height at outer wall is plotted against this parameter in Fig.9. The result is correlated fairy well in this figure. Based on the numerical results presented in Fig.9, empirical formulas for predicting the maximum wave height at the outer wall are obtained as follows:

$$\zeta_{max} = 0.79 + 1.56\alpha - 0.48\alpha^2 \tag{39}$$

5. Conclusions

A high order numerical scheme was developed for extended Boussinesq equations expressed in generalized curvilinear coordinate system. By applying it to the problem of solitary wave propagation through curved channel, the following results were obtained.

When a solitary shallow water wave propagates through a narrow circular channel, the wave is transmitted almost completely with little reflection. The shape of the transmitted wave is almost the same

(a) t=1.0

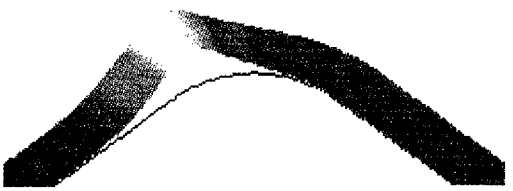

(b) t=1.2

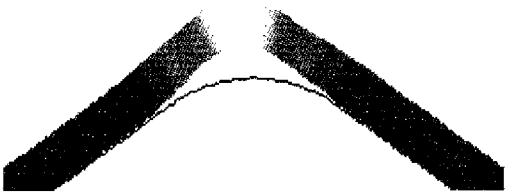

(c) t=1.4

(d) t=1.5

(e) t=1.8

Fig.4 Wave elevation at different time instants
(Case A-1, ε =0.05, $\overline{W}/\overline{h}_0$ = 5.0)

(a) t=3.3

(b) t=3.6

(c) t=3.9

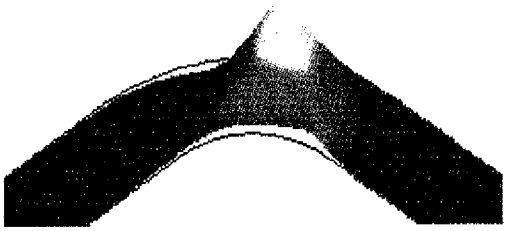

(d) t=4.2

(e) t=4.5

Fig.5 Wave elevation at different time instants
(Case B-3, ε =0.15, $\overline{W}/\overline{h}_0$ = 10.0)

(a) t=4.0

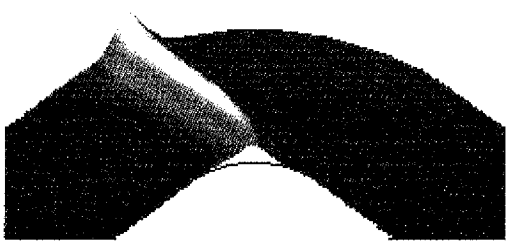

(b) t=4.4

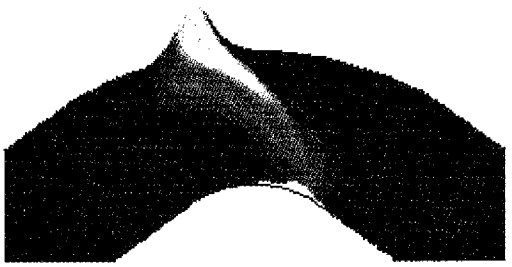

(c) t=4.8

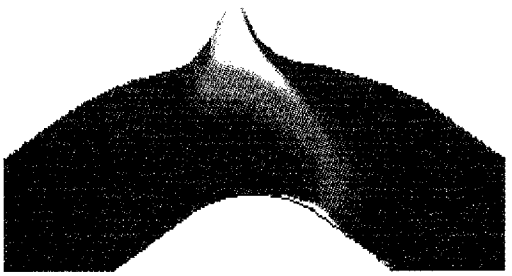

(d) t=5.0

Fig.6 Wave elevation at different time instants
(Case C-5, ε =0.25, $\overline{W}/\overline{h}_0$ = 20.0)

(e) t=5.2

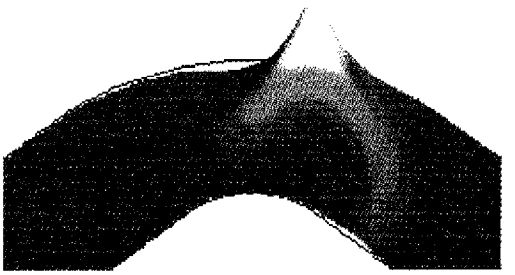

(f) t=5.4

(g) t=5.6

(h) t=6.0

Fig.6 Wave elevation at different time instants
(Case C-5, ε =0.25, $\overline{W}/\overline{h}_0$ = 20.0)

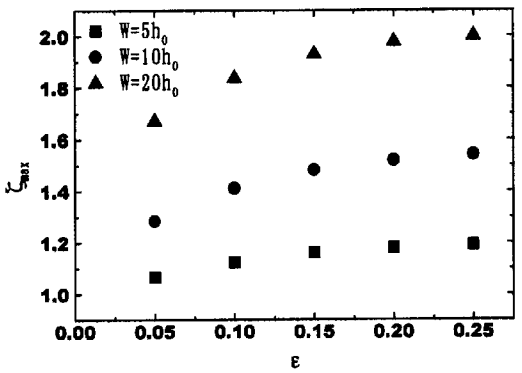

Fig.7 Maximum wave height at outer wall

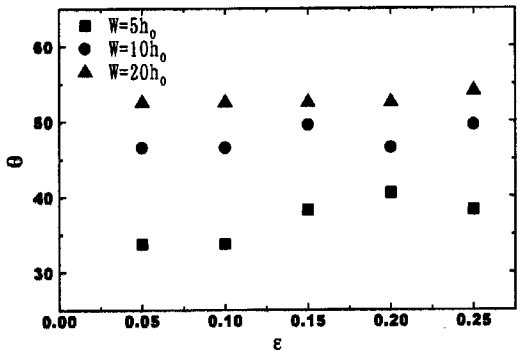

Fig.8 The location at which the maximum wave height is attained (θ is taken clockwise.)

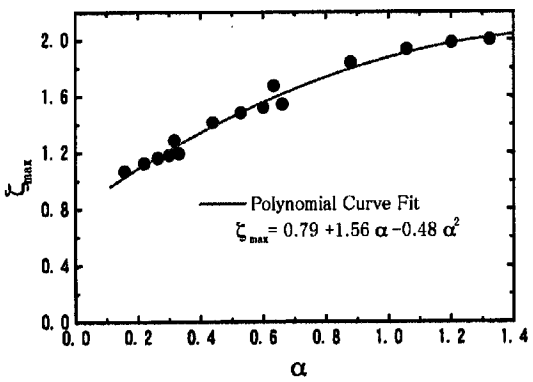

Fig.9 Maximum wave height at outer wall against the dimensionless parameter proposed by Shi et al.(1998)

as that of the incident wave. This is consistent with the results for long wave propagation in a narrow curved channel by Shi et al. (1998) .

For solitary wave traveling through a wide channel, the wave transformation is significant. In this case, the transmitted wave no longer preserves its original shape and disintegrates into several smaller waves. This is due to the combined effects of the diffraction at the corner and the lateral reflection from the outer channel wall.

The maximum wave run-up at the outer channel wall can reach almost 200% of the incident wave amplitude for wide channel. These values can be predicted fairly well with one dimensionless parameter, which was originally proposed for the straight channel with sharp-cornered 90° bend by Shi et al. (1998).

Finally, we mention that the numerical model developed in this study is applicable to the channels with more generalized geometry and bottom topography. The treatments of regular and irregular waves can also be made straightforward. Further numerical investigations are being planned.

Acknowledgments

A part of this study is supported by the fund of Disaster Prevention Research Institute, Kyoto University(Research No.8P-4 and No.10G-4).

References

Nwogu, O. (1993) : Alternative form of Boussinesq equations for nearshore wave propagation, J.Wtrwy., Port, Coast. and Oc. Engrg., Vol. 119, No.6, pp.618-638.

Press, W.H., Flannery, B.P., Teukolsky, S.A. and Vetterling, W.T. (1989) : Numerical Recipes, Cambridge University Press, Neo York, pp.569-572.

Shi, A. , Teng, M.H. and Wu, T. (1998): Propagation of solitary waves through significantly curved shallow water channels, J. Fluid Mech., Vol.362, pp.157-176.

Tanaka, M. (1993) : Mach reflection of a large-amplitude solitary wave, J. Fluid Mech., Vol.248, pp.637-661.

Wei, G. and Kirby, J.T. (1995): Time-dependent numerical code for extended Boussinesq equations, J.Wtrwy., Port, Coast., and Oc. Engrg., Vol. 121, No.5, pp.251-261.

Wei, G., Kirby, J.T., Grilli, S.T. and Subramanya, R. (1995) : A fully nonlinear Boussinesq model for surface waves. Part 1. Highly nonlinear unsteady waves, J. Fluid Mech., Vol. 294, pp.71-92.

Appendix

In this study, the non-dimensional variables are defined as follows:

$$x=\frac{\bar{x}}{\bar{\lambda}_0}, y=\frac{\bar{y}}{\bar{\lambda}_0}, z=\frac{\bar{z}}{\bar{h}_0}, t=\frac{\sqrt{\bar{g}\bar{h}_0}}{\bar{\lambda}_0} \tag{40}$$

$$u=\frac{\bar{h}_0}{\bar{a}_0\sqrt{\bar{g}\bar{h}_0}}\bar{u}, v=\frac{\bar{h}_0}{\bar{a}_0\sqrt{\bar{g}\bar{h}_0}}\bar{v} \tag{41}$$

$$\zeta=\frac{\bar{\zeta}}{\bar{a}_0}, h=\frac{\bar{h}}{\bar{h}_0} \tag{42}$$

where $\bar{g}$ =gravitational acceleration; and over-bars are used to denote dimensional valuables.

要旨

一般曲線座標系に変換された拡張型ブジネスク方程式に対する数値モデルを開発し，曲水路での孤立波の伝播解析に適用した．最初に，水路幅および入射波高が，孤立波の透過・反射特性に及ぼす影響について検討し，その特徴を明らかにした．次に，水路屈曲部における越波に関する検討項目の１つとして，外周壁面上での最大遡上高を算出し，その値がShiら（1998）の提案した無次元パラメータにより良く整理できることを示した．

キーワード：孤立波，曲水路，越波，ブジネスク方程式，座標変換